

# Surface Combustion Microengines Based on Photocatalytic Oxidations of Hydrocarbons at Room Temperature

Ming Su\*<sup>†</sup> and Vinayak P. Dravid\*

*Department of Materials Sciences and Engineering, Northwestern University, Evanston, Illinois 60208*

*Received August 8, 2005; Revised Manuscript Received September 13, 2005*

## ABSTRACT

The concept of a surface combustion microengine that is fuelled by volatile hydrocarbons at room temperature is demonstrated on a microcantilever covered with a thin layer of titanium oxide (TiO<sub>2</sub>). Exposing this microengine to ultraviolet (UV) radiation and hydrocarbon vapor produces controlled bending of the microcantilever as a result of differential stress produced by photocatalytic oxidation of organic molecules on the TiO<sub>2</sub> coating. Compared to the motion generated solely by UV radiation or hydrocarbon adsorption, the unique photocatalytic-mechanical effects in the presence of UV and hydrocarbon produce more work and exhibit fast response. The surface combustion based microengines would require less maintenance in minimally controlled field environment and could be potentially used in construction of miniature movable machines, conversion of solar and chemical energy to mechanical work, when extended to a large array of microcantilevers. We believe such microengines can be fuelled by a variety of molecules or mixtures due to the generally favorable photocatalytic reactivity of TiO<sub>2</sub>, thus potentially offering a broad approach for mechanical work generation from multiple energy sources.

The efficient generation of mechanical works from solar or fuel energy has been an active topic for many decades. Many fuel-combustion engines have been designed to improve efficiency and reduce pollution and complexity, among similar considerations. However, such engines require high-temperature combustion processes and directional heat flow to generate work. For instance internal combustion engines depend on an exothermic combustion of a mixture of hydrocarbon fuel or hydrogen and air, inside a sealed cylinder equipped with a movable piston.<sup>1</sup> Once ignited using an electrical or compression heating system, the combustion products have more available energy than the original mixture, and this energy can be translated into work by driving the piston. The remainder of the hot products are vented and the piston returns to its previous position. Any heat that is not translated to work is a waste product and removed from the engine through a cooling system. Such high-temperature combustion processes constitute inefficient engines compared to biological motors which work at room temperature in a modest environment. The adenosine triphosphate (ATP) fuelled muscle contraction is an example of mechanical work generation from chemical fuel at room temperature.<sup>2–4</sup>

The success of natural and human-made machines has attracted increasing attention for the design of miniature

machines capable of producing mechanical work from varied energy sources and platforms. In this regard, the photomechanical effects have been used to generate mechanical changes in photoisomeric molecule functionalized thin films or at the single molecular level,<sup>5–9</sup> such as nanomotors of DNA powered by enzymes, ions, DNA hybridization, and conformational changes, among others.<sup>10–17</sup> Although these examples are useful in illustrating the fundamental proof-of-concept, several challenges exist in interfacing the molecular machines to harness mechanical work, especially for solution based nanomotors that have to fight the increased degree of randomness upon the addition of fuel molecules. A hybrid molecular and solid-state micromotor has been explored in solution by covalently linking motor molecules on the surface of a microcantilever. Upon the addition of fuel, the interactions of rotaxane or its derivative and fuel generate surface stress which bends the microcantilever.<sup>18,19</sup> These advances lead to a logical question related to the traditional internal combustion engines and biological nanomotors: whether a miniature microengine fuelled by the room temperature combustion of fuel under normal atmospheric conditions can be built, and if so, will it depend on existing combustion mechanisms or on an entirely novel one? We address this intriguing possibility by demonstrating microcantilever-based photocatalytic oxidation facilitated by an active catalytic layer on the microcantilever.

Microfabricated microcantilevers have emerged as a widely used nanomechanical platform for the detection of

\* To whom correspondence should be addressed. E-mail: sum1@ornl.gov; v-dravid@northwestern.edu.

<sup>†</sup> Present address: Life Science Division, Oak Ridge National Laboratory, Oak Ridge, Tennessee 37831.

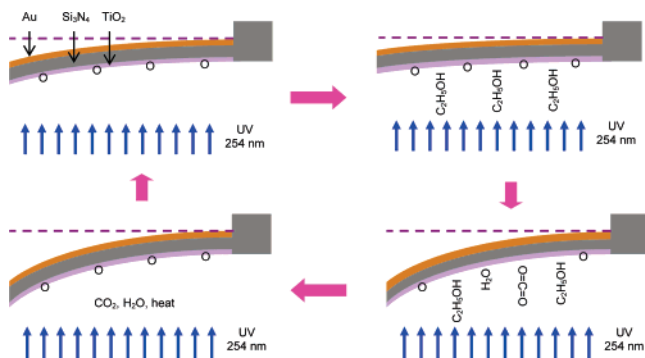


**Figure 1.** Proposed scheme for ethanol-fuelled photocatalytic microengines based on TiO<sub>2</sub> modified microcantilevers.

vapors and biomolecules, where the binding is often non-reversible and only one cycle of motion is possible.<sup>20–22</sup> To perform continuous motion in atmosphere, there has to be a mechanism to remove surface-bounded molecules and such molecules should fulfill typical constraints of thermodynamic, ergonomic, and economic considerations. Here we demonstrate a photocatalytic microengine based on the surface combustion of fuel molecules on a microcantilever coated with an active titanium oxide (TiO<sub>2</sub>) thin film. The photocatalysis of ethanol molecules on the TiO<sub>2</sub> surface in the presence of ultraviolet (UV) radiation provides the surface-stress stimulus responsible for the microcantilever bending, as well as the continuous removal of reaction products (Figure 1) for sustaining the motion. The proposed surface combustion microengine is based on a four-step process analogous to that of the four-stroke Otto cycle in internal combustion engines, namely: (1) fuel adsorption (intake), (2) UV-ignition (compression), (3) heat generation (power/combustion), and (4) surface cleaning (exhaust). The mechanical work is the output measured in the bending of the microcantilever. Briefly, the UV radiation provides a sufficient driving force for the removal of surface adsorbates resulting in bending of the microcantilever toward the light source; the fuel adsorption leads to an immediate bending away from the radiation source due to the increase in surface stress; the heat from the exothermal oxidation of fuel then bends the bimorph microcantilever; and finally the microcantilever returns to its equilibrium position after the removal of reaction products and heat. The surface adsorption and combustion-based microengine works faster and generates more mechanical work using ethanol as fuel in the presence of UV radiation than that of ethanol or UV radiation alone.

TiO<sub>2</sub> thin films are coated on microcantilevers by stepwise adsorption and hydrolysis of titanium *n*-butoxide. Commercial microcantilevers (spring constant ~0.15 N/m) from Veeco with gold reflective layers are immersed sequentially in titanium *n*-butoxide solution (100 mM in an equal molar mixture of toluene and ethanol) for 20 min to adsorb precursor, and 1 min in water to hydrolyze precursor at room temperature. The dimensions of the triangle shape microcantilevers are shown in Figure 2a. Assuming that the TiO<sub>2</sub> film will not remarkably change the spring constant of the microcantilever, the film thickness can be estimated from

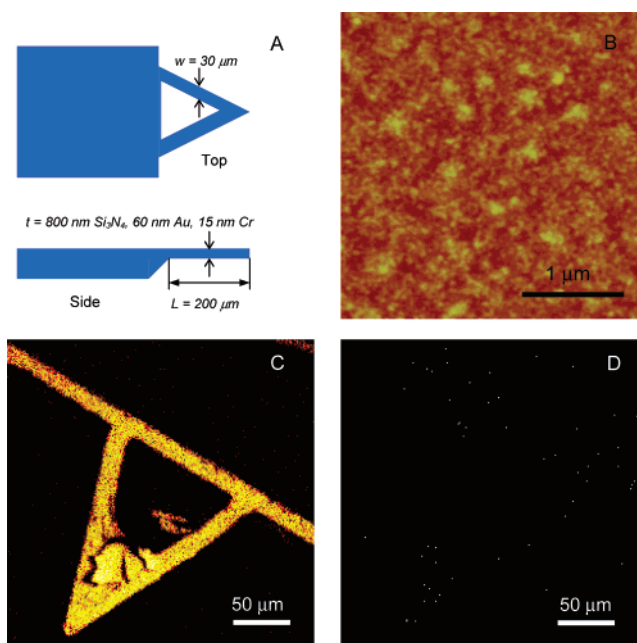


**Figure 2.** (a) Schematic illustration of dimensions of microcantilever. (b) An AFM image of a TiO<sub>2</sub> thin film deposited on a glass substrate. The elemental distribution images of a TiO<sub>2</sub> modified microcantilever collected using secondary ion signals of Ti<sup>+</sup> (c) and Si<sup>+</sup> (d).

the change in resonance frequencies before ( $f_1 \sim 160.20$  kHz) and after ( $f_2 \sim 140.23$  kHz) the coating using<sup>23</sup>

$$m = M[(f_1/f_2)^2 - 1] \quad (1)$$

The masses of Si<sub>3</sub>N<sub>4</sub> (25.6 ng), gold (11 ng) and chromium (1 ng) layers are estimated from their dimensions and densities. The geometrical considerations that usually necessitate the effective mass in the equation are canceled out, and the mass of TiO<sub>2</sub> layer is calculated to be 11.5 ng, which corresponds to a 283 nm thick film on the microcantilever. The oxide films form stable chemical bonds with the surface hydroxyl groups on the silicon nitride side as indicated in the constant frequency.<sup>24</sup> The microcantilever bending is optically monitored using the feedback electronics of an atomic force microscope (AFM, Nanoscope IIIa, Veeco). A UV lamp with radiation wavelength of 254 nm, an intensity of 0.4 mW/cm<sup>2</sup>, and a photon flux of  $0.5 \times 10^{15}$  cm<sup>2</sup>/s is used for illumination at a distance of 5 cm. The decrease in resonance frequency after TiO<sub>2</sub> thin film formation is the preliminary confirmation of surface modification. The morphology of the TiO<sub>2</sub> film formed on a glass substrate is shown in an AFM image (Figure 2b): the surface is flat with small protrusions over several micrometers. The elemental distribution on the microcantilever is confirmed using secondary ion mass spectrometry (SIMS). For SIMS, the microcantilever is intentionally broken and attached on a copper tape. The characteristic secondary ion images of Ti<sup>+</sup> (Figure 2c) and TiO<sup>+</sup> (not shown) reflect the distribution of TiO<sub>2</sub> on the microcantilever. In comparison, the contrast of the Si<sup>+</sup> image is too weak to show the shape of microcantilever and thus confirms the uniform coverage of TiO<sub>2</sub> (Figure 2d).

The photomechanical response of a TiO<sub>2</sub> coated microcantilever is studied by exposing the microcantilever to UV radiation. Although the substrate-mediated photodesorption of O<sub>2</sub> species has a threshold energy at the TiO<sub>2</sub> band gap (~3.1 eV), the exposure of the microcantilever coated with a TiO<sub>2</sub> film to UV 365 nm only bends the microcantilever slightly. However, the exposure to UV 254 nm radiation (5.1 eV) significantly bends the microcantilever toward the light source (Figure 3a). The bending reaches a saturation value in about 400 s and partially recovers when UV light is turned off. As a comparison, the exposure of a clean microcantilever without TiO<sub>2</sub> film to UV 254 nm light generates a monotonic and slow bending, and the magnitude is smaller than that of the TiO<sub>2</sub> coated microcantilever under the same conditions. Meanwhile, when the UV 254 nm radiation is periodically turned on and off with 10 s duration, the microcantilever shows a characteristic stepwise bending (Figure 3b), where the magnitude is linearly proportional to the radiation time (Figure 3b inset). The photoinduced bending is explained as the removal of surface adsorbed species such as oxygen and other adsorbates and the generation of active surface sites with unsaturated coordination.<sup>24,25</sup> The microcantilever then experiences a compressive surface stress on the UV-exposed side and a tensile stress on the other side, and thus bends toward the radiation source as the result of the stress imbalance. When the UV light is turned off, the readsorption of atmospheric O<sub>2</sub> (usually faster than other adsorbates due to the high concentration<sup>25</sup>) on active sites increases surface stress on the UV-exposed side and lead to a backward bending. The partial recovery of bending confirms the effect of other adsorbates. The photodesorption follows the first-order kinetics:  $dn/dt = -\sigma F n$  where  $n$  is the number of adsorbed O<sub>2</sub>,  $\sigma$  is the cross section of photodesorption,  $F$  is the photon flux, and  $t$  is the radiation time. The bending of the TiO<sub>2</sub> coated microcantilever with UV light in Figure 3a is fitted to  $V \sim \exp(-\sigma F t)$ , which gives a photodesorption cross section  $\sigma$  of  $2.4 \times 10^{-17}$  cm<sup>2</sup>/s. This value is close to the value of the molecular oxygen species adsorbed on the defective TiO<sub>2</sub> (100) surface ( $4.3 \times 10^{-17}$  cm<sup>2</sup>/s).<sup>26</sup> Note: any thermal effects of the UV radiation are ruled out because of the low light intensity and the following experiments with continuous UV radiation.

UV radiation of photocatalytic TiO<sub>2</sub> films creates highly reactive surfaces capable of oxidizing most organic molecules.<sup>27,28</sup> The reactivity and equilibrium bending of the TiO<sub>2</sub> coated microcantilever is maintained in continuous UV radiation and the introduction of fuel produces characteristic bending of the microcantilever. Figure 3c shows the response of the microcantilever to a 5% (v/v) mixture of ethanol vapor and air. The photodesorption cross-section ( $2.26 \times 10^{-16}$  cm<sup>2</sup>/s) is 10 times that of adsorbed molecular oxygen species, suggesting the existence of reaction products with large molecular volumes. The microcantilever bends in a unique way: an immediate bending away from the radiation, which is explained as the adsorption of ethanol on defectively active surface sites,<sup>29,30</sup> and then a bending toward the radiation source, which is explained as the thermal bending induced by the heat generated by exothermic oxidation of ethanol.

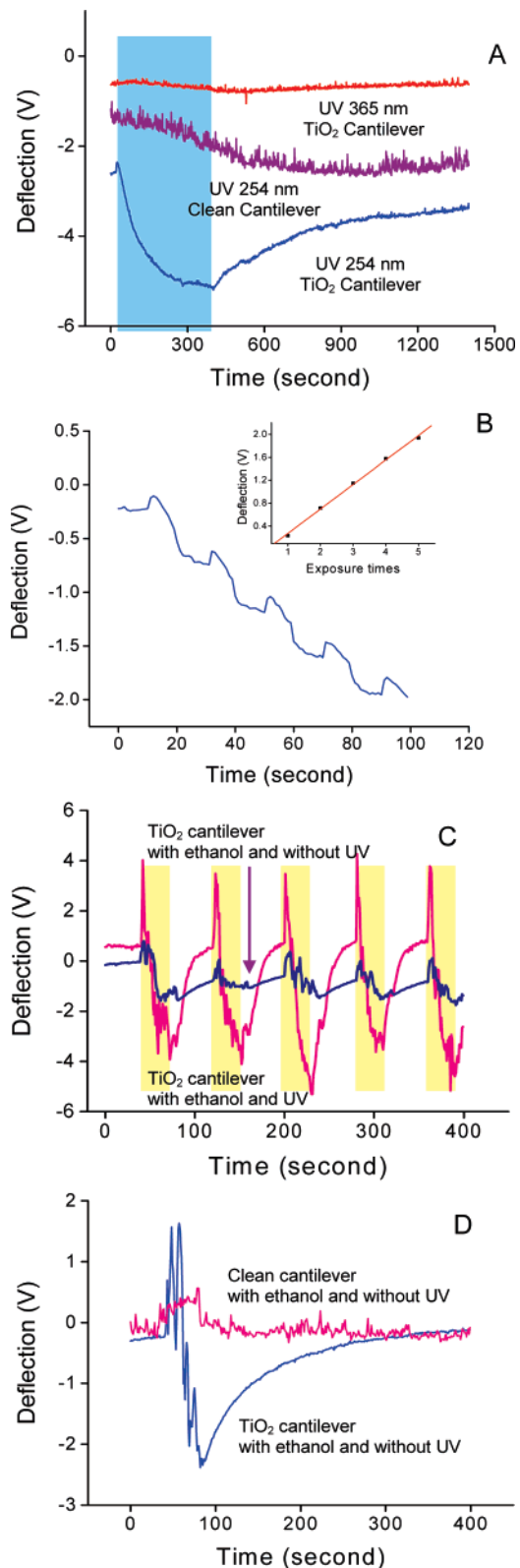


**Figure 3.** (a) Bending of a TiO<sub>2</sub> modified microcantilever exposed to UV radiations at 365 and 254 nm, and the bending of an unmodified microcantilever exposed to UV radiation at 254 nm. (b) The bending of a TiO<sub>2</sub> modified microcantilever to several periods of exposure to 254 nm UV radiation, and the relation between exposure time and the bending (inset). (c) The bending of a TiO<sub>2</sub> modified microcantilever to cycles of ethanol exposure with and without 254 nm UV radiation. (d) The bending of an unmodified microcantilever and a TiO<sub>2</sub> modified microcantilever to one cycle of ethanol vapor without the UV radiation.

The microcantilever returns to its equilibrium position in 40 s after the removal of reaction products (CO<sub>2</sub>, water, or other oxidation intermediates) and the dissipation of heat. In the control experiments with the same amount of ethanol and without UV radiation, the TiO<sub>2</sub> coated microcantilever returns to its original equilibrium position slowly and the complete recovery takes more than 200 s (Figure 3c), because of the lower catalytic ability of TiO<sub>2</sub> thin films in the dark.<sup>31</sup> The arbitrary bending magnitude with UV radiation (4.5 V) is twice that without UV radiation (2.1 V), reflecting the high bending efficiency of the UV-induced photocatalytic reaction.<sup>32–34</sup> Furthermore, the bending of a clean silicon nitride microcantilever with one side covered with gold film is monitored upon one exposure to the mixture of ethanol and air (Figure 3d), a 0.6 V bending toward the gold side is observed as the result of adsorption induced stress change. Figure 3d also shows the bending of the TiO<sub>2</sub> coated microcantilever to one cycle of ethanol exposure without UV radiation, the bending magnitude is the same as that in the cycles exposure, and clearly the full recovery takes much longer time than that in the presence of UV radiation (40 s). These control experiments confirm the high efficacy of ethanol oxidation on the TiO<sub>2</sub> coated microcantilevers in UV radiation.

The temperature change of the exothermic oxidation of hydrocarbons has not been the focus of prior studies of TiO<sub>2</sub> single crystals or colloid slurries. One possible explanation for the lack of data is that the temperature increase of surface or suspended colloids is hard to measure due to fast heat dissipation through solid bond vibrations or solvent molecules in continuous UV radiation. When the TiO<sub>2</sub> film is deposited on an ultrathin bimorph cantilever, the reaction heat from the photocatalytic oxidation can be measured through the bending of the microcantilever. The temperature increase  $\Delta T$  induced by the oxidation reaction on the microcantilever surface is calculated using the equation for the deflection  $d$  of the free-end of a bimorph cantilever in the beam theory (for simplicity the TiO<sub>2</sub> and chromium thin films are effectively treated as Si<sub>3</sub>N<sub>4</sub> and gold with a thickness of 300 and 15 nm, respectively)<sup>35</sup>

$$d = \frac{L^2}{h_1} \frac{3(1+m)}{[3(1+m)^2 + (1+mn)(m^2 + 1/mn)]} (\alpha_1 - \alpha_2) \Delta T \quad (2)$$

where subscripts 1 and 2 denote Si<sub>3</sub>N<sub>4</sub>-TiO<sub>2</sub> and gold-chromium layer;  $\alpha$  is the thermal expansion coefficient ( $3 \times 10^{-6} \text{ K}^{-1}$  for Si<sub>3</sub>N<sub>4</sub> and  $14.2 \times 10^{-6} \text{ K}^{-1}$  for gold);  $n = E_1/E_2$ , with  $E$  Young's moduli (250 GPa for Si<sub>3</sub>N<sub>4</sub> and 78 GPa for gold);  $m = h_1/h_2$ ,  $h_1$  is the thickness of Si<sub>3</sub>N<sub>4</sub>-TiO<sub>2</sub> layer (1.08  $\mu\text{m}$ ) that consists of 800 nm Si<sub>3</sub>N<sub>4</sub> and 283 nm TiO<sub>2</sub>, and  $h_2$  is the thickness of gold-chromium layer that consists of 60 nm gold and 15 nm chromium;  $L$  is the length of the cantilever (200  $\mu\text{m}$ ). The substitution of Si<sub>3</sub>N<sub>4</sub> for TiO<sub>2</sub> will not introduce much difference considering their thermal expansion coefficients ( $3 \times 10^{-6} \text{ K}^{-1}$  for Si<sub>3</sub>N<sub>4</sub> and  $7 \times 10^{-6} \text{ K}^{-1}$  for rutile TiO<sub>2</sub>), Young's moduli (250 GPa for Si<sub>3</sub>N<sub>4</sub>

and 286 for TiO<sub>2</sub>), and the fact that amorphous materials usually have smaller values for both properties than bulk crystals.

The bending in the presence of ethanol vapor and UV radiation generates an average voltage change of 6.4 V in the photodetector output, which corresponds to a vertical displacement of 82 nm at the end of the microcantilever with the piezotube sensitivity in the  $z$  direction of 12.8 nm/V. The temperature increase is 44.9 °C as calculated using eq 2. If the surface combustion of ethanol is adiabatic, the heat produced on the TiO<sub>2</sub> surface is calculated as 1148.09 nJ after considering the mass of each layer and the specific heat of Si<sub>3</sub>N<sub>4</sub> (0.69 J/g °C), TiO<sub>2</sub> (0.52 J/g °C), gold (0.129 J/g °C), and chromium (0.45 J/g °C). There is considerable evidence which suggests that ethanol oxidation on TiO<sub>2</sub> is a multistep reaction through various intermediates, including acetaldehyde and formaldehyde to final product of CO<sub>2</sub>.<sup>36,37</sup> To generate 1148.09 nJ of heat, at least 0.26 ng of ethanol has to be oxidized to acetaldehyde or 0.038 ng to CO<sub>2</sub>. Since the saturation coverage of ethanol on the TiO<sub>2</sub> anatase surface is 3.0–3.2 molecules/nm<sup>2</sup>,<sup>2,37</sup> at least 17.8 layers of ethanol ( $5.1 \times 10^{11}$  molecules) have to be oxidized to CO<sub>2</sub> in order to generate the 82 nm vertical displacement at the end of the microcantilever, providing the active area equals the surface area ( $9.53 \times 10^3 \mu\text{m}^2$ ) of the microcantilever. In addition, the overall energy efficiency cannot be derived from the current experiment because the amount of consumed ethanol and the degree of oxidation cannot be determined. However, the energy efficiency and the fraction of contribution from UV radiation can be obtained through a correlation with those of a similarly prepared large area TiO<sub>2</sub> surface, where the consumed ethanol and the product distribution can be determined using other instruments such as mass spectrometry.

Finite element analysis (FEA) was used to calculate the force and work generated on the microcantilever using the commercial software Abaqus 6.4 (Hibbit Karlsson Sorensen Inc.). The boundary condition is applied for the FEA of the microcantilever, in which the end is fixed and the vertical displacement is applied at the free end, step by step, following the movement path of the free end. The vertical displacement is derived from the microcantilever deflection output and the sensitivity of the piezotube in the  $z$  direction. The external work is calculated as reaction force and moment at each increment multiplied by the according displacement and rotation. A Young's modulus of 250 GPa and a Poisson's ratio of 0.3 are used for silicon nitride. In view of their small thickness and stiffness, the gold layer and TiO<sub>2</sub> thin film are not taken into account in the numerical simulations. The compressive and tensile force acting on the bottom side and the top side of the microcantilever are shown in Figure 4a. The net result is the cantilever bending as a result of force (stress) imbalance. Figure 4b shows the time dependent changes of mechanical work (regardless of the bending direction) derived from the bending of the TiO<sub>2</sub> coated microcantilever in three situations: ethanol alone, UV radiation, and ethanol vapor in the presence of UV radiation. UV radiation produces a similar amount of work as that of

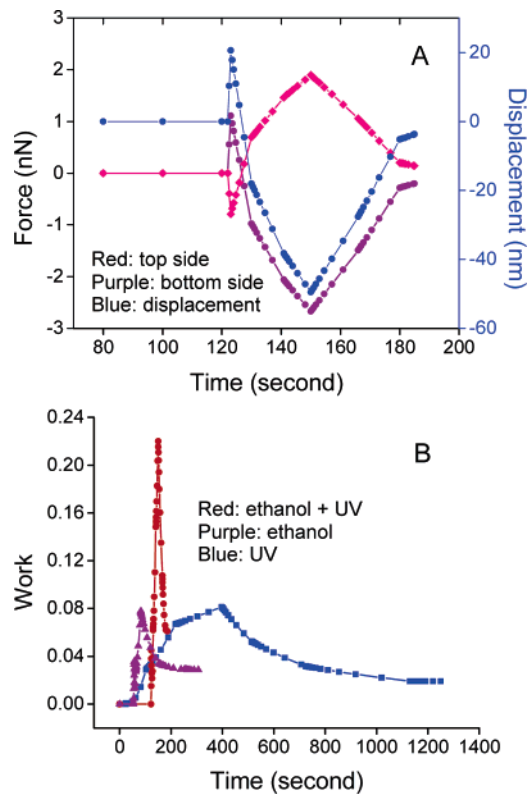


**Figure 4.** (a) Compressive stress, tensile stress, and net force acting on a TiO<sub>2</sub> modified microcantilever in one ethanol exposure with UV radiation at 254 nm. (b) The mechanical works as a function of time generated by the TiO<sub>2</sub> modified microcantilever at different situations: pure ethanol, UV alone, ethanol and UV together.

ethanol alone; however, the work produced by ethanol in the presence of UV is almost three times larger than that of UV or ethanol alone.

Intuitively, the microengine described here should be classified as an open cycle engine which is usually less powerful than internal combustion engines where the fuel–air mixtures are pressed to high pressures before ignition. The successful demonstration of the photocatalytic microengine actually suggests the possibility to construct a novel locomotive based on the surface adsorption and surface combustion of fuel on a modified microcantilevers or beams. The efficiency of such microengines should be compared to that of similar-sized internal combustion engines, or to test whether the same idea can be applied directly to drive large scale motion.

We have demonstrated an ethanol-fuelled microengine on a photocatalytic film coated microcantilever, which has several advantages compared to traditional internal combustion engines and previously reported miniature motors. (1) The photocatalytic and self-clean ability of TiO<sub>2</sub> enable the application of diversified energy sources including organic vapors, simple gases, and arbitrary mixtures, regardless of their purity. (2) The well-established knowledge of TiO<sub>2</sub> offers room for property enhancement through proper doping and structural modifications, and for potential industrial-scale production using economically attractive synthesis approaches. (3) The fabrication and modification methods are well-established to fabricate massively parallel microcanti-

lever arrays with small mass and active photocatalytic coatings that can potentially offer high power-to-weight ratio, increased efficiency, and additional feasibility for the conversion of solar and chemical energy to mechanical work at large scale.

**Acknowledgment.** The NU work was supported primarily by the Nanoscale Science and Engineering Initiative of the National Science Foundation under NSF Award No. EEC-0118025 and the Air Force Office of Scientific Research through a Multiple University Research Initiative under Contact No. F49620-00-1-0283. We thank Dr. Hui Shen at the Department of Mechanical Engineering of NU for the finite element analysis. M.S. thanks Wigner fellowship program at ORNL for support. The Oak Ridge National Laboratory is managed by UT-Battelle for the U.S. Department of Energy under Contract No. DE-AC05-00OR22725.

## References

- (1) Obert, E. F. *Internal combustion engine: analysis and practice*; International Textbook Co.: Great Britain, 1950.
- (2) Vale, R. D.; Milligan, R. A. *Science* **2000**, *288*, 88.
- (3) Kuo, S. C.; Sheetz, M. P. *Science* **1993**, *260*, 232.
- (4) Kelly, T. R.; De Silva, H.; Silva, R. A. *Nature* **1999**, *401*, 150.
- (5) Koumura, N.; Zijlstra, R. W. J.; van Delden, R. A.; Harada, N.; Feringa, B. L. *Nature* **1999**, *401*, 152.
- (6) Yu, L.; Nakano, M.; Ikeda, T. *Nature* **2003**, *425*, 145.
- (7) Ikeda, T.; Nakano, M.; Yu, Y. L.; Tsutsumi, O.; Kanazawa, A. *Adv. Mater.* **2003**, *15*, 201.
- (8) Hugel, T.; Holland, N. B.; Cattani, A.; Moroder, L.; Seitz, M.; Gaub, H. E. *Science* **2002**, *296*, 1103.
- (9) Saha, S.; Johansson, L. E.; Flood, A. H.; Tseng, H.-R.; Zink, J. I.; Stoddart, J. F. *Small* **2005**, *1*, 87.
- (10) Yan, H.; Zhang, X. P.; Shen, Z. Y.; Seeman, N. C. *Nature* **2002**, *415*, 62.
- (11) Simmel, F. C.; Dittmer, W. U. *Small* **2005**, *1*, 284.
- (12) Li, J. W. J.; Tan, W. H. *Nano Lett.* **2002**, *2*, 315.
- (13) Seeman, N. C. *Trends Biochem. Sci.* **2005**, *30*, 119.
- (14) Chen, Y.; Lee, S. H.; Mao, C. *Angew. Chem.* **2004**, *43*, 5335.
- (15) Dittmer, W. U.; Simmel, F. C. *Nano Lett.* **2004**, *4*, 689.
- (16) ALberti, P.; Mergny, J. L. *Proc. Natl. Acad. Sci.* **2003**, *100*, 1569.
- (17) Yurke, B.; Turberfield, A. J.; Mills, A. P.; Simmel, F. C.; Neumann, J. L. *Nature* **2000**, *406*, 605.
- (18) Huang, T. J.; Tseng, H.-R.; Sha, L.; Lu, W.; Brough, B.; Flood, A. H.; Yu, B.-D.; Celestre, P. C.; Chang, J. P.; Stoddart, J. F.; Ho, C.-M. *Nano Lett.* **2004**, *4*, 2065.
- (19) Liu, Y.; Flood, A. H.; Stoddart, J. F. *J. Am. Chem. Soc.* **2004**, *126*, 9150.
- (20) Chen, G. Y.; Thundat, T.; Wachter, E. A.; Warmack, R. J. *J. Appl. Phys.* **1995**, *77*, 3618.
- (21) Fritz, J.; Baller, M. K.; Lang, H. P.; Rothuizen, H.; Vettiger, P.; Meyer, E.; Guntherodt, H.-J.; Gerber, C.; Gimzewski, J. K. *Science* **2000**, *288*, 316.
- (22) Wu, G. H.; Datar, R. H.; Hansen, K. M.; Thundat, T.; Cote, R. J.; Majumdar, A. *Nat. Biotechnol.* **2001**, *19*, 856.
- (23) Cleveland, J. P.; Manne, S.; Bocek, D.; Hansma, P. K. *Rev. Sci. Instrum.* **1993**, *64*, 403.
- (24) Kovtyukhova, N. I.; Buzaneva, E. V.; Waraksa, C. C.; Martin, B. R.; Mallouk, T. E. *Chem. Mater.* **2000**, *12*, 383.
- (25) Lu, G.; Linsebigler, A.; Yates, J. T. *J. Chem. Phys.* **1995**, *102*, 4657.
- (26) Rusu, C. N.; Yates, J. T. *Langmuir* **1997**, *13*, 4311.
- (27) Hoffmann, M. R.; Martin, S. T.; Choi, W.; Bahnemann, D. W. *Chem. Rev.* **1995**, *95*, 69.
- (28) Mor, G. K.; Carvalho, M. A.; Varghese, O. K.; Pishko, M. V.; Grimes, C. A. *J. Mater. Res.* **2004**, *19*, 628.
- (29) Schaub, R.; Thosttrup, P.; Lopez, N.; Lagsgaard, E.; Stensgaard, I.; Norskov, J. K.; Besenbacher, F. *Phys. Rev. Lett.* **2001**, *87*, 266104.
- (30) Liu, G.; Rodriguez, J. A.; Chang, Z.; Hrbek, J. J. *Phys. Chem. B* **2002**, *106*, 9883.

- (31) Linsebigler, A. L.; Lu, G.; Yates, J. T., Jr. *Chem. Rev.* **1995**, *95*, 735.
- (32) Pilkenton, S.; Hwang, S.-J.; Raftery, D. J. *J. Phys. Chem. B* **1999**, *103*, 11152.
- (33) Varghese, O. K.; Malhotra, L. K.; Sharma, G. L. *Sens. Actuators B* **1999**, *55*, 161.
- (34) Muggli, D. S.; McCue, J. T.; Falconer, J. L. *J. Catal.* **1998**, *173*, 470.
- (35) Yang, J. P.; Deng, X. C.; Chong, T. C. *J. Micromech. Microeng.* **2005**, *15*, 958.
- (36) Lusvardi, V. S.; Barteau, M. A.; Farneth, W. E. *J. Catal.* **1995**, *153*, 41.
- (37) Kim, K. S.; Barteau, M. A.; Farneth, W. E. *Langmuir* **1988**, *4*, 533.

NL0515605